# MEASUREMENT AND MODELLING OF AN UWB CHANNEL AT HOSPITAL

L. Hentilä[1], A. Taparungssanagorn, H. Viittala and M. Hämäläinen
Centre for Wireless Communications
P.O. Box 4500, FI-90014 University of Oulu, Finland
Email: {lhentila, pong, hviittal, mattih}@ee.oulu.fi

***Abstract* - This paper describes the results of an ultra wideband (UWB) channel measurements and modelling from 3.1 to 6.0 GHz carried out at the Oulu University Hospital. Mainly line-of-sight (LOS) channels were measured having transmitter-receiver separation from 3 to 6 m. The modelling is done in time domain and in frequency domain, and the results are compared with. Channel parameters that are corresponding to the modified Saleh-Valenzuela (SV) model in time domain and autoregressive (AR) model in frequency domain are extracted from the measurement data. Also, delay spreads and path losses are examined. In the study, the effect of the huge frequency diversity over the UWB band on the path loss is pointed out.**

## I. INTRODUCTION

The performance prediction and simulation of new communication systems based on the UWB technology require a deep knowledge of a physical radio channel. Most of the recent measurements that have been carried out to characterise the UWB channel are based on the frequency domain approach, whereas the modelling has been done in time domain [1, 2]. In this paper, the modelling is emphasized in time domain but also frequency domain autoregressive (AR)-modelling is pointed out. The paper is organised as follows. Section II presents the measurement setup and the experiment procedure. Section III describes the parameters of the measurement environment. Section IV describes the channel modelling in time domain and section V in frequency domain. Finally, section VI concludes the paper.

## II. MEASUREMENT SETUP

The channel measurement system used in this work is presented in detail in [3]. The sounder consists of a vector network analyser Agilent 8720ES (VNA), a wideband amplifiers, a wideband conical antenna pair ARA CMA-118/A, coaxial cables and a control computer as illustrated in Figure 1. In addition, a stepped track is used to enable antenna movement. Table 1 lists the main parameters of the measurements.

The frequency band used in the measurements is from 3.1 GHz to 6.0 GHz, giving a bandwidth of 2.9 GHz. The measured band falls inside the Federal Communications Committee (FCC) spectrum mask for UWB transmission that is from 3.1 GHz to 10.6 GHz [4]. The maximum number of frequency points per sweep is limited by the VNA to 1601.

In order to enhance the antenna positioning accuracy, a stepped track (antenna carriage) is used in the RX-end. During the measurements, the control PC instructs the RX antenna carriage to move along the rail with 5.0 cm steps. The length of the track is 2.5 m providing 50 separate antenna positions. TX antenna is kept in a fixed position throughout the measurement of one track position. Antenna heights in both ends were 1.4 m above the floor.

A system calibration was made to compensate the frequency dependent variation and attenuation caused by the adapters and cables. Effective isotropic radiated power (EIRP) is calculated taking all the losses and gains into account. 20 sweeps are recorded at each antenna location. The RX-antenna carriage positions were determined by measuring distances to walls using a laser ranging device whose measurement accuracy is typically 3 mm.

The reference measurement was performed in an anechoic chamber at the University of Oulu. The impulse response of the sounder was extracted in the channel modelling phase by reducing the free space loss (at distance 1 m) from the reference measurement and compensating the result of each measured sweep in the raw data.

Table 1. Measurement setup parameters

| **Parameter** | **Value** |
|---|---|
| Frequency band | 3.1 to 6.0 GHz |
| Bandwidth | 2.9 GHz |
| Number of points within the band | 1601 |
| Sweep time | 800 ms |
| Average noise floor | –90 dBm |
| Tx power (amplifier output) | +21 dBm |
| Amplifier gain (avg.) | 32 dB |
| Antenna gain (typical) | 0 dBi |
| TX cable loss (max) | 6 dB |
| RX cable loss (max) | 15 dB |
| EIRP (min) | 0 dBm = 1 mW |

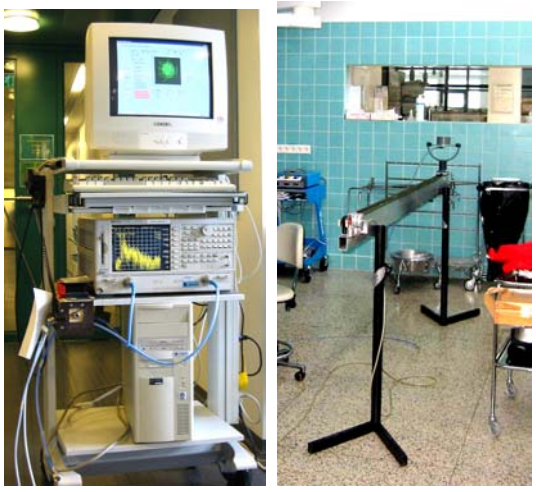

Figure 1. The measurement setup: a trolley and the antenna on the carriage.

[1] Currently with Elektrobit Ltd., Oulu, Finland.

0-7803-9398-8/05/$20.00 ©2005 IEEE

## III. Environmental Parameters

The channel measurements presented in this document have been carried out at the Oulu University Hospital. The measured environments were operating room, x-ray examination room and intensive care unit (ICU). Except for ICU, there was no movement inside a room when recording the data. As an example, measurement layout in operating room is shown in Figure 2.

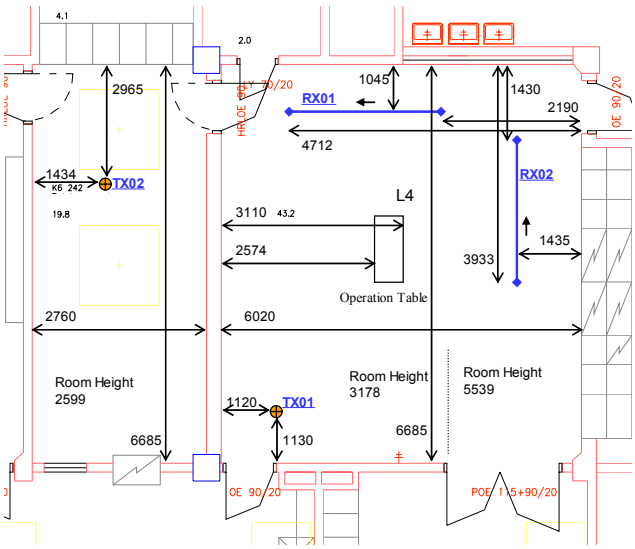


Figure 2. Layout of the operating room and the used antenna positions.

The main wall material of the operating room was concrete. There were some chromium plated working tables in this room. The walls in x-ray examination room were thick leaded concrete having two leaded windows. Environment in ICU was quite close to a typical laboratory room or big office.

## IV. Time Domain Analysis

The recorded data was stored in a polar format, i.e., in complex numbers. Firstly in the post-processing, the frequency domain raw data was inverse Fourier transformed to the time domain for the further analysis. The time domain data contains impulse responses of the measured radio channels. All the signals detected during the measurement campaign at different rooms and positions are used to obtain the power delay profiles (PDP) of each position. PDPs are the basis of the time domain analysis.

Windowing (Hamming) was used to obtain the arrival time of the first path in the PDP, but the channel model parameters are extracted without windowing.

For all impulse responses, normalisation is performed by setting the channel energy at each position to unity such that the area under each PDP is equal to one. The normalised impulse response $IR_n$ is obtained by

$$IR_n = \frac{h(t)}{\sqrt{\sum_{k=1}^{L} |h(t_k)|^2}}. \qquad (1)$$

The PDP is then a squared value of the $IR_n$. The normalisation makes it possible to compare the statistics of the PDPs that have been measured at different positions.

### A. Channel Characteristics

RMS delay spread, mean excess delay and number of paths within 10 dB of the maximum peak are obtained from the measurement data. RMS delay spread is a time domain parameter which is typically used to give an idea of the channel's characteristics.

The time domain parameters are obtained from the PDPs by taking into account the thresholds presented in Figure 3 for LOS link. Before delay domain analysis, the initial delay (propagation delay) is removed first. The most accurate way to find the initial delay is to compare the exact distance measured with the laser ranging device and the position of the corresponding path from the measured data. The average noise level is typically around 50 dB below the maximum multipath component in the normalised PDP, but it is estimated separately for all the cases by averaging the measured data before the first multipath component arrives [7]. RMS delay spread and mean excess delay are then calculated from the data, which is 15 dB above the noise level. Approximately 35 dB dynamic range is then obtained for the final channel modelling.

RMS delay seemed to be typically between 10 ns and 17 ns in indoor environments.

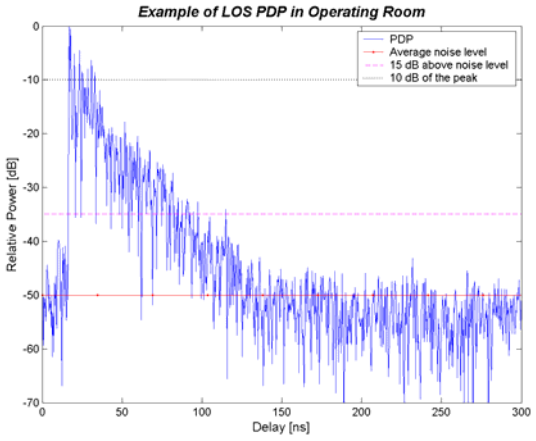


Figure 3. Typical PDP in LOS channel in the operating room.

Channel characteristics extracted from the measurement data are tabulated in Table 2. In Figure 4, cumulative distribution functions (CDF) of the calculated RMS delay spreads are shown for each room.

Table 2. Channel characteristics

| | Operating Room | | | X-ray Examination Room | | | Intensive Care Unit | | |
|---|---|---|---|---|---|---|---|---|---|
| Meas. position | 1 | 2 | 3 | 4 | 5 | 6 | 7 | 8 | 9 |
| $\tau_m$ [ns] | 10.4 | 16.7 | 31.3 | 16.1 | 16.0 | 40.2 | 15.0 | 14.1 | 10.4 |
| $\tau_{RMS}$ [ns] | 10.8 | 11.9 | 11.4 | 15.1 | 15.7 | 15.5 | 17.4 | 15.3 | 10.8 |
| $NP_{10\,dB}$ | 13 | 18 | 19 | 13 | 16 | 41 | 9 | 9 | 13 |
| $NP_{85\,\%}$ | 29 | 42 | 60 | 50 | 56 | 75 | 38 | 38 | 29 |

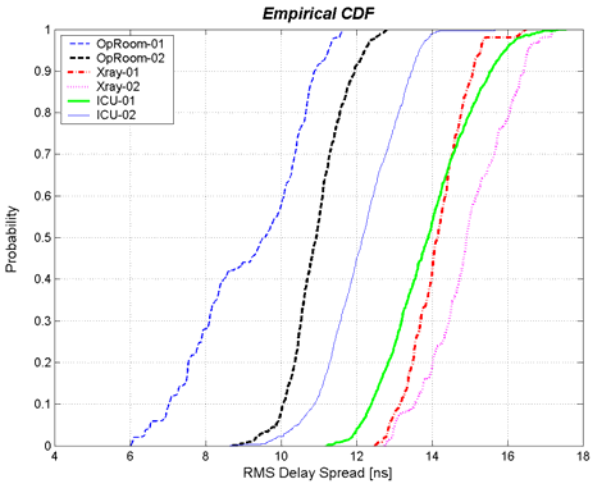


Figure 4. CDFs of RMS delay spread.

### B. *Multipath Amplitude Fading*

Small-scale statistics include multipath amplitude fading analysis. Data was gathered from the PDP's of different environments and positions. Amplitudes smaller than 20 dB of the peak in the PDP were set to zero in order to get only the appropriate data for the analysis. Extraction of the amplitudes for each tap was carried out by collecting a vector of 100 amplitude values having an equivalent delay. 80 taps in the operating room and in the intensive care unit and 120 taps in the x-ray examination room fitted inside the 20 dB threshold. The small-scale area contains one room and 100 measurement positions. The candidate amplitude distributions named Nakagami, Gamma, Rice, Rayleigh and Lognormal were tested using a Kolmogorov-Smirnov's goodness-of-fit test. A significance level of 5% was used to evaluate the reliability of the fit. Figure 5 presents the result of the test in operating room. Table 3 shows the results of the entire test in all the measured environments. Nakagami seems to fit best to the data but Lognormal is very close the same.

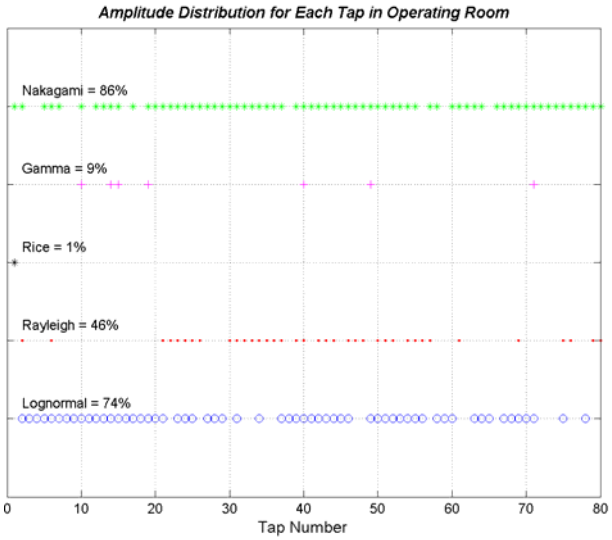


Figure 5. Amplitude distributions for each tap depicting operating room. Percent values express the amount of taps which follow the given distribution.

Table 3. Pass rates of multipath fading distributions

| Distribution / Room | **Operating Room** | **X-ray Examin. Room** | **Intensive Care Unit** |
|---|---|---|---|
| Nakagami-m (%) | 86 | 89 | 86 |
| Gamma (%) | 9 | 14 | 14 |
| Rice (%) | 1 | 1 | 1 |
| Rayleigh (%) | 46 | 70 | 59 |
| Lognormal (%) | 74 | 88 | 78 |

### C. *Multipath Modelling*

The multipath model is obtained by investigating the multipath propagated signals in the PDP. The proposed model for the channel having the cluster phenomenon is a modified IEEE 802.15.3a model defined in [9]. The model presented in [10] is modified in order to fit the measured UWB channel data to the model. Even if the Nakagami-m distribution fitted best to the amplitude fading statistics there is no reason to modify the SV-model since the lognormal distribution fitted also well. Table 4 shows the parameters which have been extracted from the measurement data and are modifying the parameters of IEEE 802.15.3a channel model from [9]. Values from the table can be used to generate channel realizations for simulation purposes using the original Matlab code, e.g., from [9].

Table 4. Modified IEEE 802.15.3a model parameters and simulated and measured channel characteristics reflecting the channel at the hospital

| **Model Parameters** | **Operating room** | | **X-ray room** | | **Intensive care unit** | |
|---|---|---|---|---|---|---|
| $\Lambda$ [1/ns] | 0.04 | | 0.05 | | 0.09 | |
| $\lambda$ [1/ns] | 2 | | 1.5 | | 2 | |
| $\Gamma$ [ns] | 9 | | 13.3 | | 16 | |
| $\gamma_r$ [ns] | 8 | | 10 | | 5 | |
| $\sigma_1$, $\sigma_2$ [dB] | 3.4 | | 3.4 | | 3.4 | |
| $\sigma_x$ [dB] | 1.5 | | 1.5 | | 1.5 | |
| **Model Characteristics** | Meas | Sim | Meas | Sim | Meas | Sim |
| $\tau_m$ [ns] | 10.4 | 10.4 | 16.1 | 16.3 | 15.0 | 15.6 |
| $\tau_{RMS}$ [ns] | 10.8 | 10.1 | 15.1 | 15.0 | 17.4 | 15.7 |
| $NP_{10\,dB}$ | 16 | 16 | 15 | 19 | 9 | 16 |
| $NP_{85\,\%}$ | 36 | 27 | 53 | 37 | 38 | 33 |

Figure 6 compares an averaged PDP from the measurements in the operating room and corresponding simulated version of the PDP. One hundred realizations have been averaged to the figure.

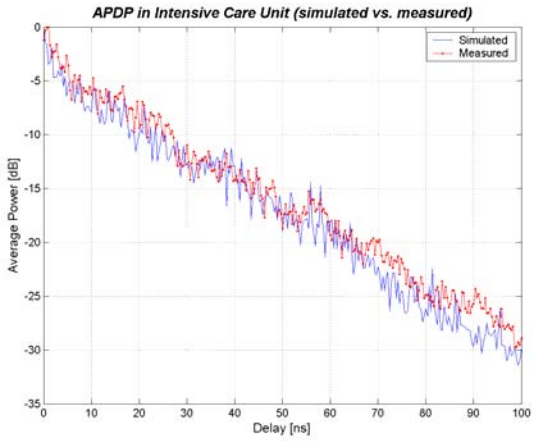


Figure 6. Average normalised PDP: simulated versus measured.

## V. Frequency Domain Analysis

### A. Path Loss

The path loss is calculated by averaging the transfer function over the frequency band as a function of distance as [8]

$$PL(d) = -10\log_{10}\left(\frac{1}{1601}\sum_{i=1}^{1601}|H(d,f_i)|^2\right), \qquad (2)$$

where $H(f_i)$ is a channel transfer function.

Path loss presented in Figure 7 proves that indoor UWB LOS radio channel can have path loss exponent below the free space loss, i.e., two. This can be explained by the fact that indoor UWB radio channel is very rich of reflected signals who gains the received signal.

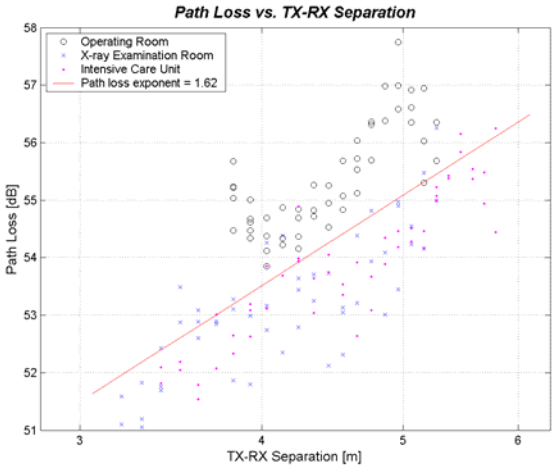


Figure 7. Path losses for different rooms.

### B. Autoregressive Modelling

The measured samples of the frequency response $H(f_n,x)$ can be interpreted as a random process. The autocorrelation function of this process is [11]

$$R(k,x) = \frac{1}{N}\sum_{i=1}^{N-k} H^*(f_i,x)H(f_{i-k},x),\ k \geq 0. \qquad (3)$$

This function provides the average received power ( $p_r = R(0,x)$ ), and it is used in autoregressive (AR) modelling to solve the channel model parameters. The frequency response can be interpreted as the output of the autoregressive process. AR modelling of time series data used for spectral estimation and the techniques for determination of the coefficients of the AR process are well known in the literature [11, 12]. With AR process assumption and non-stationary assumption of the channel, the frequency response at each location is a realization of an autoregressive process of order $m$ given by [11-13]

$$H(f_n,x) + \sum_{i=1}^{p} a_i H(f_{n-i},x) = e(f_n), \qquad (4)$$

where $H(f_n,x)$ is the $n^{\text{th}}$ sample of the complex frequency domain measurement at location $x$ and $\{e(f_n)\}$ is a complex white noise process. The parameters of the model are complex constants $a_i$. Taking the z-transformation of (4), AR process can be depicted as an output of a linear filter with transfer function [11]

$$G(z) = \frac{1}{1+\sum_{i=1}^{p} a_i z^{-1}} = \prod_{i=1}^{p}\frac{1}{(1-p_i z^{-1})}, \qquad (5)$$

driven by a white noise process $\{e(f_n)\}$ [11]. Using AR model, the channel frequency response which was represented by $N$ samples will be identified with $p$ parameters of the AR model or the location of $p$ poles of the $G(z)$ where typically $N >> p$. The channel poles are given by $z_i = e^{j2\pi f_i T_s}$, where $T_s$ is the sampling time. The Doppler frequency $f_i$ of the $i^{th}$ path at the receiver is caused by the movement of the mobile terminal or scatterers.

The AR parameters $\{a_i\}$ are the solution of the Yule-Walker equation [11]

$$R(-l) + \sum_{i=1}^{p} a_i R(i-l) = 0, \qquad (6)$$

where $R(l) = R(l,x)$ is frequency correlation function defined in (3). The variance of the zero mean white noise $\{e(f_n)\}$ is the same as the minimum mean error of the predictor, which is given by [11]

$$\sigma_v^2 = R(0) + \sum_{i=1}^{p} a_i R(i). \qquad (7)$$

In this case, modelling explains that a pole close to the unit circle represents significant power at the delay related to the angle of the pole. The delay can be calculated as

$$\tau_i = \arg(p_i)/2\pi f_s\,. \qquad (8)$$

The model order selection criteria explained in [13-15] are examined to determine the conservative estimate of the order of the process. Two important criteria, Akaike Information-theoretic Criterion (or an Information-theoretic criterion) (AIC) proposed in [13-15] and Minimum Description Length Criterion (MDL) proposed in [16], which are shown as

$$AIC(k) = \log(\hat{\sigma}_k^2) + 2\frac{k}{N} \qquad (9)$$

and

$$MDL(k) = \log(\hat{\sigma}_k^2) + \frac{k}{N}\log(N) \qquad (10)$$

have been adopted in this study. By applying these criteria to many measured frequency responses, it is concluded that a 5th order process is sufficient to represent the statistics of the channel model.

For a 5th order model applied to the data from the operating room, the magnitude of the largest pole was $p_1$ = 0.89, the second pole was $p_2$ = 0.79 and the magnitudes of the remaining poles $p_{3\text{-}5}$ = ~0.4, which are relatively smaller than the first two poles. Figure 8 illustrates the complex z-plane scattering plot of a time-varying 5th order AR model for the data measured at the operating room.

The arrivals of the significant paths are then 18.8 ns and 48.9 ns, respectively, which correspond to the angular range of -0.068π and -0.177π, respectively. Figure 9 shows the average normalised PDP obtained by taking the inverse Fourier transform of the frequency response re-

generated from the AR model using 100 channel realizations and the modified IEEE 802.15.3a model. Figure 10 illustrates the CDF of the RMS delay spreads in the operating room to confirm that the regenerating models are close statistical fits to the measurement data.

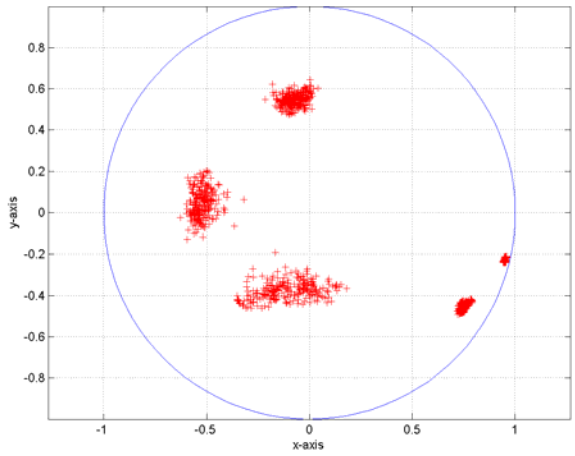


Figure 8. The complex z-plane scatter plot of an AR model of order 5 for experiment.

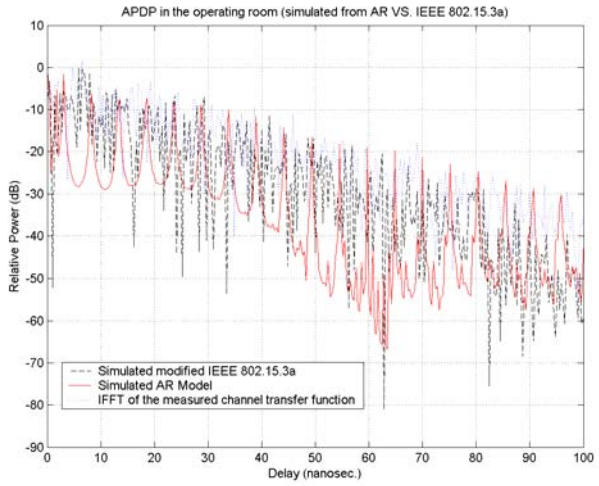


Figure 9. Average normalised PDP: simulated from the AR versus measured.

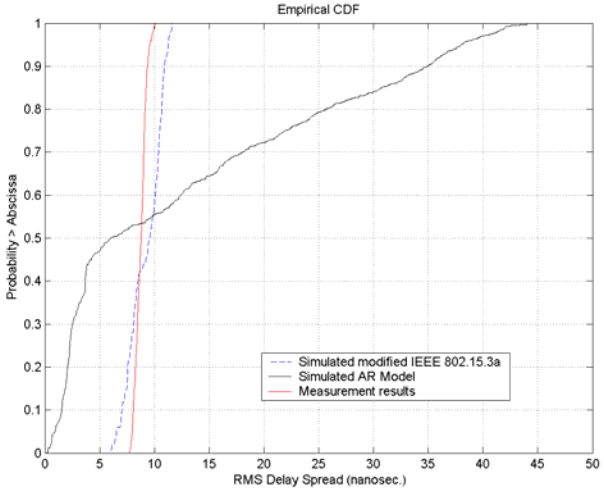


Figure 10. CDF of the RMS delay spreads in the operating room.

## CONCLUSIONS

The multipath indoor channel models for hospital have been obtained from the measured data by investigating the average power delay profiles of different environments. The modifications of IEEE 802.15.3a channel model that is based on the Saleh-Valenzuela channel model have been constructed. A statistical autoregressive model for simulation of indoor UWB radio channel was also described. The AR model is simpler than the existing time domain models due to the fewer parameters needed. The location of each pole of the AR model represented cluster of arrival paths. The angle of the pole represented the arrival time and the closeness to the unit circle indicates the strength of the cluster. A five pole model was shown to be sufficient to regenerate the statistical characteristics of the radio channels. The accuracies of the methods are analyzed by comparing the channel characteristics and the cumulative distribution functions of the RMS delay spread.

## ACKNOWLEDGMENTS

The authors would like to thank the National Technology Agency of Finland (Tekes), the Finnish Defence Forces and Elektrobit for funding this research.

## REFERENCES

[1] M.Z. Win and R.A, Scholtz, "Characterization of Ultra-wide Bandwidth Wireless Indoor Communications Channel, A communication theoretic view," *IEEE J. Select. Areas Commun.,* Vol. 20, No. 9, pp. 1613–1627, Dec 2002.

[2] R.J. Cramer, R.A. Scholtz and M.Z. Win, "An Evaluation of the Ultra-Wideband Propagation Channel," *IEEE Trans. Antennas Propagat.,* Vol. 50, No 5, pp. 561–570, May 2002.

[3] M. Hämäläinen, T. Pätsi and V. Hovinen, "Ultra Wideband Indoor Radio Channel Measurements," *Proc. of the 2nd Finnish Wireless Communications Workshop*, Tampere, Finland, 2001.

[4] Federal Communication Commission, *"The First Report and Order Regarding Ultra-Wideband Transmission Systems*," FCC 02-48, ET Docket No. 98-153, 2002.

[5] J. Keignart and N. Daniele, "Channel Sounding and Modelling for Indoor UWB Communications," *Proc. of the First International Workshop on Ultra Wideband Systems*, Oulu, Finland, 2003.

[6] R. Vaughan and J. B. Andersen, "*Channels, Propagation and Antennas for Mobile Communications*," The IEE Electromagnetic Waves Series 50, London, 2003.

[7] D. Cassioli, M.Z. Win and A.F. Molisch, "The Ultra-Wide Bandwidth Indoor Channel: From Statistical Model to Simulations," *IEEE J. Select. Areas Commun.*, Vol. 20, No. 6, pp. 1247 – 1257, Aug. 2002.

[8] S.S. Ghassemzadeh, L.J. Greenstein, A. Kavčić, T. Sveinsson and V. Tarokh, "An Empirical Indoor Path Loss Model for Ultra-Wideband Channels," *KICS Journal of Communications and Networks*, Vol. 5, No. 4, 2003.

[9] J. Foerster, "*Channel Modelling Sub-committee; Final Report*". IEEE P802.15-02/490r1-SG3a, Mar 2003.

[10] A.A.M. Saleh and R.A. Valenzuela, "A Statistical Model for Indoor Multipath Propagation," *IEEE J. Select. Areas Commun.*, Vol. 5, pp. 128 – 137, Feb 1987.

[11] S. Haykin, "*Adaptive Filter Theory*," 4th Edition, Prentice Hall.

[12] S. Lawrence Marple, Jr., "*Digital Spectral Analysis*", Prentice Hall, Signal Processing Series, 1987.

[13] S.J. Howard and K. Pahlavan, "Autoregressive Modeling of Wide-Band Indoor Radio Propagation," *IEEE Trans. Commun.*, Vol. 40, No. 9, pp. 1540 – 1552, Sep 1992.

[14] H. Akaike, "A new look at the statistical model identification," *IEEE Trans. Automat. Contr.*, Vol. 19, Issue 6, Dec 1974.

[15] H. Akaike, "Use of statistical models for time series analysis," *IEEE International Conf. on Acoustics, Speech, and Signal Processing*, Vol. 11, pp. 3147 – 3155, Tokyo, Japan, 1986.

[16] B. Aksasse and L. Radouane, "Two-dimensional autoregressive (2-D AR) model order estimation," *IEEE Trans. Signal Processing*, Vol. 47, Issue. 7, pp. 2072 – 2077, July 1999.